Mechanism of photocatalytic bacterial inactivation on TiO₂ films involving cell-wall damage and lysis

C. Pulgarin [a,1,2], J. Kiwi [a,*,1], V. Nadtochenko [b,1,3]

[a] Ecole Polytechnique Fédéral de Lausanne, EPFL-SB-ISIC-GGEC, Lausanne 1015, Switzerland
[b] Institute of Problems of Chemical Physics (RAS), Semeneov Av. 1, Chernogolovka, Moscow Region 142432, Russia

ARTICLE INFO

ABSTRACT

This article addresses the cell wall damage of *Escherichia coli* (from now on *E. coli*) by TiO₂ suspensions. The dynamics of TiO₂ photocatalysis by thin films layers is described. The films were characterized by FTIR spectroscopy and atomic force microscopy (AFM). The *E. coli* complete inactivation is shown to be due to the partial damage of the cell-wall components (peroxidation). A small increase in the cell wall disorder concomitant with a decrease of the cell wall functional groups leads to higher cell wall fluidity as the precursor step preceding cell lysis.

© 2012 Elsevier B.V. All rights reserved.

1. Introduction

TiO₂ mediated disinfection has been reported since 1988 to be possible against bacteria, viruses, fungi and algae [1–3].

The EPFL group has worked for years in the bacterial degradation by TiO₂ powders, suspensions, colloids and TiO₂ supported on textiles and thin plastic films. The catalytic activity of commercial TiO₂ powders for the abatement of *Escherichia coli* under solar simulated light on many commercial powders with different BET areas and isoelectric points (IEP) was recently reported [4]. Rincon and Pulgarin have reported the effect of continuous and intermittent light intensity of suspensions/supported TiO₂ during *E. coli* abatement [5–7].

The *E. coli* used throughout this work had the size of 1 μm and a 75 Å cell envelope including the more resistant peptoglycan (PGN) layer. It includes 35×10^6 molecules of polysaccharides (PLS) and phosphatidyl-ethanolamine (PE) which is the main protein of *E. coli* amounting to 60% the total protein content.

TiO₂ however has several limitations as a photocatalyst, which inhibit a more extensive utilization in commercial applications. A major limitation is the lack of response of TiO₂ to visible light since it requires UV-light ≤ 390 nm for photo-activation. This means that TiO₂ photocatalysis utilizes only 4% of the incoming solar energy.

To extend its adsorption into the range of the solar spectrum, sol–gels of TiO₂ are prepared with N- and S has been used extensively in our laboratory [8–10]. The doped films inactivated *E. coli* but the efficiency of the N,S-TiO₂ doped materials was an order magnitude below non-doped TiO₂ and therefore not suitable at the present time for practical applications. This is the very reason to use highly oxidizing Ag, Cu metal nanoparticle in conjunction with TiO₂ to attain a faster bacterial inactivation by hybrid-semiconductor materials [11–15]. The fact that Ag, Cu trap the TiO₂ electron under light enhancing the charge separation is another argument to add metal nanoparticles with possible beneficial effects when harvesting solar light with disinfecting hybrid composites.

The dynamics and mechanism of *E. coli* inactivation using TiO₂ under solar simulated irradiation have been reported by various studies [16–19]. FTIR and AFM were used to quantify the degradation of the cell-wall components of *E. coli*. The incoming light used was >340 nm, above the threshold absorption of *E. coli* protein bilayer ensuring that all the light was absorbed by the TiO₂.

2. Experimental

2.1. TiO₂ porous film preparation

The 8 μm TiO₂ film was prepared by mixing TiO₂ Degussa P25 powder (50 m²/g) from Degussa Ag, Hanau, Germany with poly (ethylene-glycol) using TiO₂ 100 g/l and PEG-2000 30 g/l. The PEG is widely used in the preparation of TiO₂ suspensions since it is known to increase the coating fluidity on a variety of surfaces and also avoids partially the agglomeration of the TiO₂ particles. This mix was spread on a microscope glass using the strip blade

* Corresponding author. Tel.: +41 21 693 36 21; fax: +41 21 693 41 11.
E-mail addresses: cesar.pulgarin@epfl.ch (C. Pulgarin), John.Kiwi@epfl.ch (J. Kiwi), nadtochenko@gmil.com (V. Nadtochenko).
[1] These authors contributed equally to this work.
[2] Fax: +41 21 693 5690.
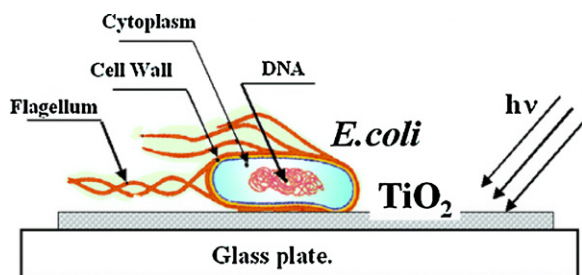[3] Fax: +7 96 524 9676.

Fig. 1. *E. coli* deposited on TiO$_2$ films as described in Section 2.

technique. The film was then dried in air for 20 min. The PG-2000 was burned-off in a flow of oxygen at 400 °C during 0.5 h. No organic contamination was detected by FTIR on the TiO$_2$ porous films prepared according to this procedure. Non-semiconductor Al$_2$O$_3$ porous films were prepared from the mixture of the Al$_2$O$_3$ powder with poly-(ethylene glycol). The set-up for the 8 μm Degussa TiO$_2$ porous film on the glass is shown in Fig. 1. *E. coli* was oxidized on the surface of the thin porous Degussa P-25 films.

E. coli in the form of small unilamellar vesicles (SUV) layers were deposited on porous TiO$_2$ films fixed on microscope glass by dipping in TiO$_2$ suspension for 3 h and then washed doubly using distilled water. The data presented in this study refer to FTIR SUV on TiO$_2$/glass and *E. coli* on TiO$_2$ glass [18].

The SUV layers were prepared by the following procedure: (1) the *E. coli* film was spread on the surface of the TiO$_2$ coated glass, (2) transformation of the film on the glass into a multi-lamellar vesicle suspension by stirring the vesicle solution (10 mg/ml) with Raschig glass rings under N$_2$ purging leading to a turbid solution and (3) ultrasonication of the solution containing the multi-lamellar vesicles with N$_2$ until a transparent colloid of unilamellar vesicles was obtained.

Fully hydrated samples of *E. coli* were irradiated with Philips BL UV-A 4 × 18 W, 4 mW/cm^2 luminescent lamps in the spectral region between 340 and 400 nm (max at 366 nm) and the compartment of a Suntest solar light simulator from Heraeus, Hanau, Germany at 37 °C.

2.2. FTIR-spectroscopy

The infrared spectra were measured in a Portmann Instruments spectrophotometer equipped with a Specac attachment (45° one pass diamond crystal). Spectra were the results of 256 scans Fourier deconvolution and second derivative of the spectral bands were used to quantify the ATR-FTIR peaks by Fourier deconvolution. To fit the complex bands Lorentzian, Gaussian, or Voigt functions were used. For the solutions requiring optical transparency, the supernatant fraction after sedimentation after 20 days of TiO$_2$ Degussa P25 was used. In addition, some experiments were performed with a semitransparent porous TiO$_2$ film on a glass plate, loading subsequently the TiO$_2$ porous film with the selected vesicle.

After the ATR-FTIR scans, the samples were dried in vacuum oven overnight and ATR-FTIR scans were repeated. The infrared spectra of the samples were sensitive to hydration since a difference was observed between hydrated and dry-samples. ATR-FTIR spectra of hydrated or dry samples were employed to monitor the peroxidation of *E. coli* but showed the same peaks for hydrated or dry samples.

2.3. Inactivation of E. coli K12

The samples of *Escherichia coli* (*E. coli* K12) were obtained from the Deutsche Sammlung von Mikroorganismen und Zellkulturen GmbH (DSMZ) ATCC23716, Braunschweig, Germany. TiO$_2$ films were deposited on glass slides. The dimensions of these glass slides

were 2 cm × 2 cm. The glass slides was sterilized by autoclaving at 121 °C for 2 h with a 20 μl aliquot of the culture with an initial concentration of 3.8 × 10^6 CFU ml^{-1} in NaCl/KCl. The samples were placed on a Petri dish provided with a lid to prevent evaporation. After each determination, the sample was transferred into a sterile 2 ml Eppendorf tube containing 1 ml autoclaved NaCS/KCl saline solution. This solution was subsequently mixed thoroughly using a Vortex for 3 min. Serial dilutions were made in NaCl/KCl solution. A 100-μl sample of each dilution was pipetted onto a nutrient agar plate and then spread over the surface of the plate using the standard plate method.

2.4. Atomic force microscopy (AFM) experiments

Measurements were performed with a Parks Scientific XE120 AFM in contact mode. The Cantilever used was an Olympus OMCL-TR400 with a spring constant 0.02 N/m. Several images were taken within a scanning field 5 μm × 5 μm were taken using a line frequency 2 Hz. Images were flatten along the *X*-axis, line-by-line by means of a 2nd order polynomial expression and the roughness was calculated using Parks' XEI software. The samples for the AFM images were prepared mixing 100 μl *E. coli* with the slurry of TiO$_2$ and applying the mixture drop-wise on the glass before drying.

3. Results and discussion

Fig. 2 shows changes in intensity and integral absorbance of ATR-FTIR spectra of *E. coli* due to the photocatalytic treatment on TiO$_2$.

ATR-FTIR peaks of *E. coli* were assigned to functional groups in *E. coli* in Figs. 2 and 3 [20]: (1) between 3000 and 2800 cm^{-1} is assigned to C–H stretching vibrations of –CH$_3$ and –CH$_2$. The weak band near 3010 cm^{-1} is due to the =C–H group (unsaturated fatty acid chains), (2) between 1800 and 1500 cm^{-1} is due mainly to amide I and amide II bands, (3) nucleic acids bands show up in the 1590–1490 cm^{-1} region owing to amino-acid side-chain vibrations, (4) between 1500 and 1300 cm^{-1} bands arise from –CH$_2$ and –CH$_3$ bending modes of lipids and proteins. At ∼1400 cm^{-1} a stretching vibrations of –COO$^-$ carboxylic group band was observed, (5) P=O double bonds and asymmetric stretching vibrations of phosphodiester/monoester phosphate are observed around 1230 cm^{-1}, (6) the region between 1200 and 900 cm^{-1} shows the symmetric stretching for C–O–P of oligo/polysaccharides. The TiO$_2$ films by themselves show a shoulder near 1000 cm^{-1} due to the lattice vibrations of TiO$_2$. A band of 1640 cm^{-1} with the width (FWHM) 96 cm^{-1} of the H$_2$O on the TiO$_2$ surface; a wide skewed band in the region 3270–2600 cm^{-1} with a maximum ∼3380 cm^{-1} due to the OH vibrations of the absorbed water and a weak narrow band near 3698 cm^{-1} due to OH groups on the TiO$_2$ surface [21].

Fig. 2a reveals significant changes in the *E. coli* spectra during photocatalysis such as: the disappearance of amide A ∼3295 cm^{-1}, amide B ∼3060 cm^{-1}. Also the disappearance of C–H bands at 2963 cm^{-1}, 2927 cm^{-1}, 2872 cm^{-1}, 2852 cm^{-1} after 960 min were observed. Concomitantly, the wide band containing the OH-vibrations changes to a skewed form with a maximum at 3480 cm^{-1}. Fig. 2b shows significant changes for the initial oligosaccharide bands around 1087 cm^{-1} at times around 45 min, along changes of the profile of the PO$_2^-$ bands near 1242 cm^{-1}, as well as the decay of the amide I band near 1653 cm^{-1} and the amide II at 1545 cm^{-1}. In parallel, a rise of the absorbance of C=O bonds of aldehydes and ketones between 1680 and 1750 cm^{-1} was observed. Beyond 120 min (Fig. 2b), the most prominent peaks are seen at 1410 cm^{-1} and 1370 cm^{-1} due to the increase in the concentration of carboxylic groups.

Fig. 3 presents the enhanced resolution of the Fourier deconvoluted spectra between 1800 and 940 cm^{-1} for the data reported in Fig. 2b. About 30 *E. coli* spectral bands were resolved by
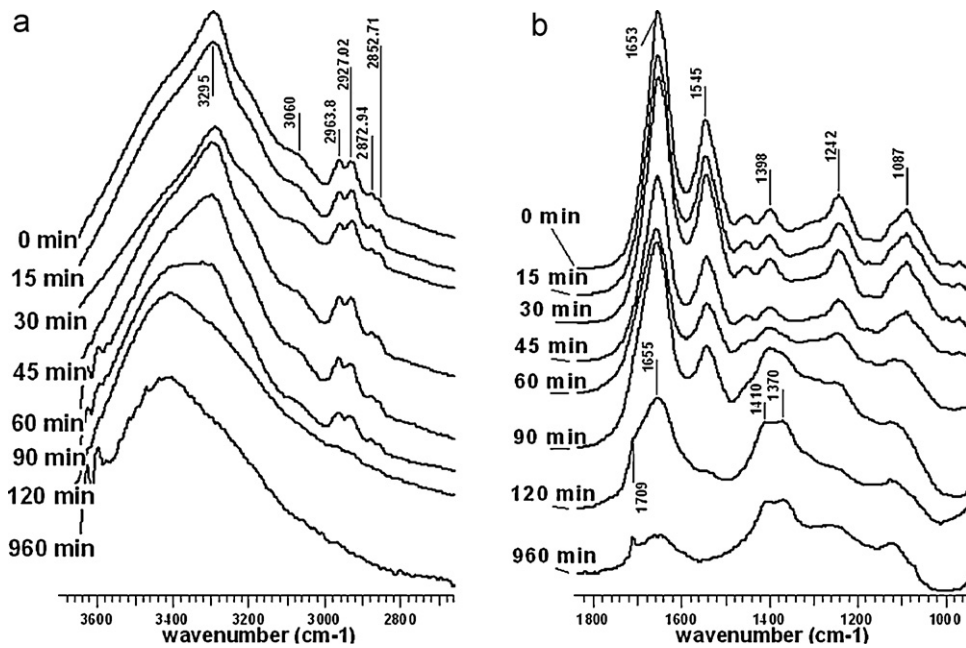
Fig. 2. Normalized ATR-FTIR spectra of *E. coli* at the TiO$_2$ film interface, during light irradiation with a BLB source. Spectra of dry samples are shown. (a) Bands in the spectral region 3700–2650 cm^{-1}, (b) bands in the spectral region 1850–950 cm^{-1}. For other experimental details see text.

deconvolution and the second-derivative was used to find the exact peak positions. For instance, the amide I band of 1653 cm^{-1}, in Fig. 2b (one band) was resolved into separate peaks at: 1655 cm^{-1}, two peaks for β-sheet at 1687 cm^{-1} and an additional β-sheet peak of 1635 cm^{-1} [22]. It was also observed that the intensities of the amide I band peaks at 1684 cm^{-1}, 1656 cm^{-1}, and 1633 cm^{-1} as well as the intensities of the two amide II peaks at 1546 cm^{-1} and 1517 cm^{-1} change within times > 30 min indicating a structure change of the proteins in the *E. coli* cell. Changes in the profile of PO$_2^-$ bands near 1244 cm^{-1} and 1215 cm^{-1} were observed in Fig. 3, due to hydrogen phosphate group being broken [24]. Third, the shapes of oligosaccharide bands 1110–950 cm^{-1} were seen to be substantially decreased during the first 30–60 min irradiation. All these lead to damage of *E. coli* due to: peroxidation involving C=O peaks that appear during the formation of COO$^-$ groups and α,β-unsaturated aldehydes that appear during the breakdown of hydroperoxides [17,18].

The formation of peroxidation products like aldehydes, ketones, and carboxylic acids is detected in the parallel to the vanishing of

features of the constituents of the cell wall membranes [16]. The FTIR spectra found for the peroxidation products of *E. coli*, and SUV reveal numerous features related to the appearance of oxidation products due to the photocatalytic activity of TiO$_2$ on sugar rings, lipid chains and polypeptide molecules of *E. coli* and acyl chains of SUV.

The ATR-FTIR data about SUV on TiO$_2$ surface suggest the introduction of disorder of the SUV lipid layer during the photocatalysis that leads to SUV peroxidation. The peroxidation of SUV on TiO$_2$ is faster compared to *E. coli* cell, suggesting that the order of the SUV bilayer structure determines the rate of the photocatalytic peroxidation process. A shift of the >CH$_2$ stretching bonds was also observed during photocatalysis. This shift seems to be the precursor of the structural changes in the cell wall membranes during lipid peroxidation.
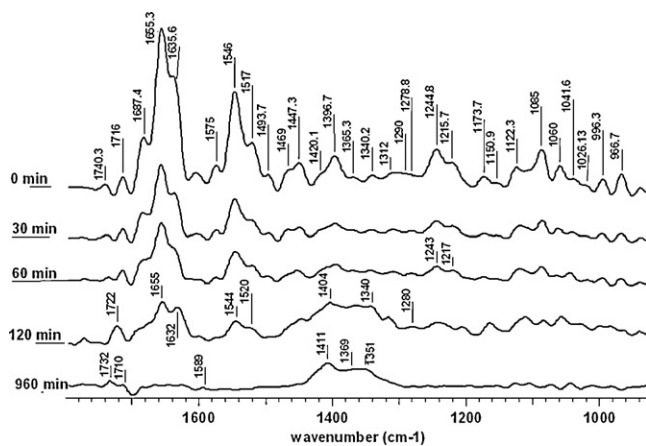

Fig. 3. Deconvoluted ATR-FTIR spectra of *E. coli* in the region 1800–950 cm^{-1}. Non-normalized data irradiated on TiO$_2$ up to 960 min. The deconvolution procedure used half-width = 21.893 cm^{-1} and Bessel apodization.
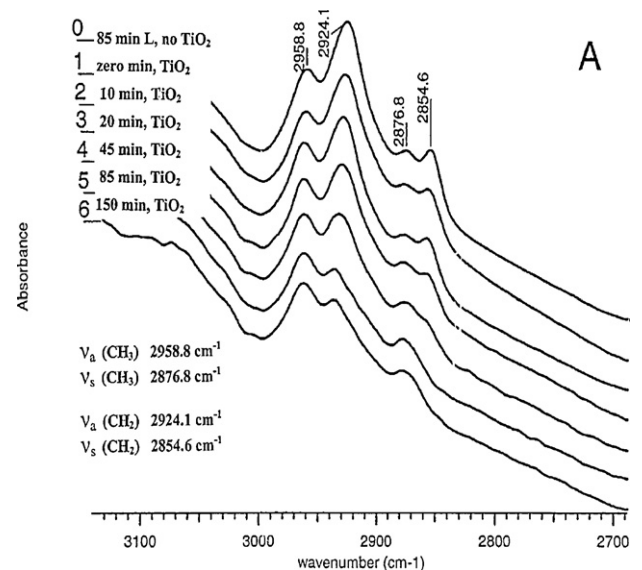

Fig. 4. FTIR spectra of *E. coli* irradiated by Suntest simulated solar light in the presence of TiO$_2$ up to 150 min irradiation time.
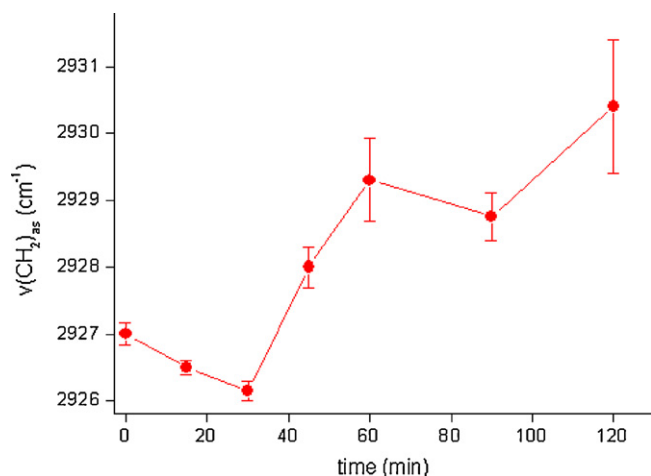
Fig. 5. Dependence of the symmetric —CH$_2$ vibration band position as a function of irradiation time using a Suntest solar simulated light for theTiO$_2$ photocatalytic mediated *E. coli* inactivation.

Fig. 6. Left hand side: AFM images before irradiation with TiO$_2$ Degussa-P25 (1 mg/1 ml) and right hand side control experiment after 1 h under the same conditions. The middle scheme shows the implosion in the last stage of the photocatalysis leading to *E. coli* lysis.

Fig. 4 shows the spectra of *E. coli* during photocatalytic treatment in the presence of TiO$_2$ under Suntest solar source in the region 3100–2700 cm^{-1}. The vibrational modes symmetric and asymmetric for the —CH$_3$— and —CH$_2$— vibrational stretching bands changes during photocatalysis between 0 and 150 min. About 70% of the *E. coli* cell wall mass is made by this type of bonds and this is why we focus on these functional groups [17]. Changes in the packing of the cell wall layers have been reported in relation to the spectral changes shown in Fig. 4 [16]. The results shown in Fig. 4 show the dependence of the symmetric —CH$_2$ band peak position as a function of irradiation time. This is shown in more detail in Fig. 5.

Fig. 5 shows that the peak position changes from 2926 to 2931 cm^{-1} after 1-h irradiation. This change leads to an increase in the cell-wall bilayer fluidity since *E. coli* is sensitive to changes in the cell wall components. Information on the lipid acyl chains has been mainly extracted from the frequency maximum and bandwidth of the C—H$_2$ stretching vibrations [25]. These vibrations are related to localized bonds not directly involved in the isomerization of the carbon backbone, but appear to be sensitive to chain order. Vibrational spectra are sensitive to alterations in the conformation and dynamics of the lipid acyl chains so that the technique may be used to monitor lipid phase behavior directly without the possibility of structural perturbations induced by probe molecules.

For the three bilayer cell walls of *E. coli*: lipo-polysacccharide (LPS), phosphatidyl-ethanolamine (PE) and peptoglycan (PGN), the cell-wall structure and fluidity have been reported to be sensitive to the peroxidation reported in Figs. 1 and 2 [24]. The blue shift of the bands in Fig. 5 indicates the increase in fluidity associated with structural modifications involving an increase in intermolecular distances.

Fig. 6 shows the irradiated and non-irradiated AFM micrographs of *E. coli* exposed to Suntest light photocatalyzed by TiO$_2$. The survival kinetics showed a decrease in the number of *E. coli* cells from 2.7×10^7 CFU/ml at time 0 to 8×10^6 CFU/ml after 30 min and to 7×10^5 CFU/ml after 1 h and to 10^2 CFU/ml after 2 h irradiation. Control experiments in the absence of TiO$_2$ but under light irradiation showed a bacterial survival of 2×10^7 CFU/ml after 1 h and 1×10^7 after 2 h. If the bacterial full inactivation is due to bacterial lysis then the AFM data in Fig. 6 agree with the survival kinetics showing that the *E. coli* concentration decreases about 35 times within 1 h.

In separate experiments not described hereby [22–25] the main three bilayer cell walls of *E. coli*: lipo-polysacccharide (LPS), phosphatidyl-ethanolamine (PE) and peptoglycan (PGN) show
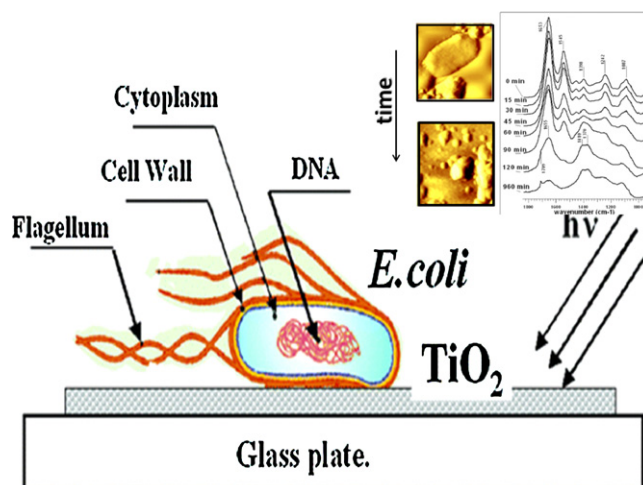
complete or almost complete disappearance when photocatalytic TiO$_2$ irradiations were carried out for 0.5 h, 1–2 h, and 40–44 h, respectively. Since the *E. coli* under light on TiO$_2$ occurred within 1–2 h the attack by the TiO$_2$ generated species, h$^+_{v.b.}$, e$^-_{c.b.}$, OH^o, HO$_2$ or radical ROS-species proceed through a collective mechanism of *E. coli* inactivation. A collective mechanism means that PGN that needs 40–44 h irradiation is oxidized much faster in *E. coli* than when is irradiated alone. This means that the radicals formed during the PE and LPS oxidation participate in the oxidation of PGN.

In the middle section in Fig. 6, the implosion of the cell wall occurs when a small amount of damage occurs in the functional components of the bacterial cell walls (Figs. 2 and 3). The high solute concentration inside the cell wall creates a pressure of 4.8 atm within the bacterial wall envelope (see Fig. 6), the solution inside the damaged bacterial wall will burst and flow out to equilibrate with the outside media by osmosis.
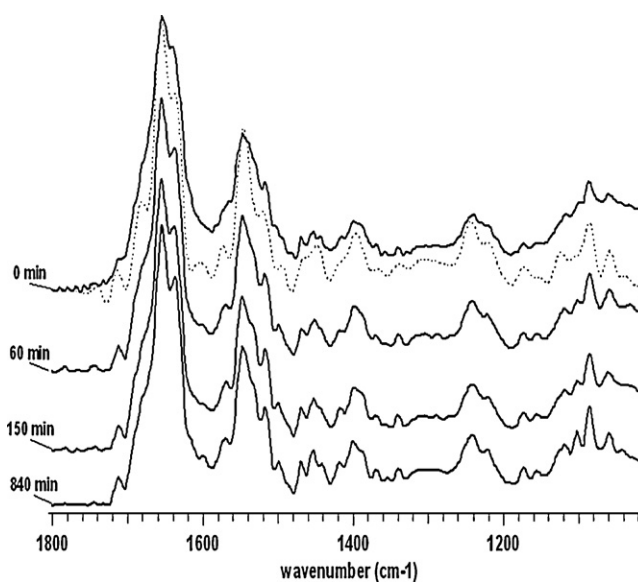

Fig. 7. Deconvoluted ATR-FTIR spectra of *E. coli* on Al$_2$O$_3$ porous film at different irradiation times up to 840 min using a BLB light source. Dashed line at $t = 0$ min. The *E. coli* ATR-FTIR spectra are shown on the TiO$_2$ surface. Bessel apodization was applied.

Figs. 2 and 3 present the *E. coli* photocatalytic degradation on a TiO$_2$ thin film. A more detailed analysis of the changes in the main functional components is shown in Figs. 4 and 5. Concomitantly, an increase in the cell wall fluidity was observed (Fig. 5) leading ultimately to *E. coli* lysis (Fig. 6). Therefore, a cell wall barrier is necessary to keep an internal constant environment: biomolecules, salts and pH. The *E. coli* survival depends on the stability of this internal environment. The existence of several bands of the cell walls by ATR-FTIR at longer times beyond the *E. coli* lysis provides the experimental evidence that low levels of peroxidation are only needed for *E. coli* inactivation. After 1–2 h photocatalysis, the time of *E. coli* inactivation, the functional groups of PE and PGN bilayers are still present indicating that proteins (PE) and polysaccharides (LPS) are not completely oxidized.

Fig. 7 shows the results of control experiments when non-semiconductor Al$_2$O$_3$ porous films (bg 7.3 eV) used during *E. coli* irradiation. Almost no changes were observed in the FTIR spectra of *E. coli* after 840 min irradiation and only small changes in amide I and amide II bands were detected. This is a proof for the photocatalytic nature of the *E. coli* peroxidation occurring on the TiO$_2$ thin films (TiO$_2$ 3.1 eV).

4. Conclusions

- The destruction of *E. coli* cell-wall bilayers at the TiO$_2$ porous film was followed by FTIR, focusing on the main functional groups in the bilayers. The decrease of these functional groups occurred with the simultaneous appearance of aldehydes, ketones and carboxylic acids.
- FTIR, AFM and the cell viability data show that *E. coli* during photocatalysis mediated by TiO$_2$ films undergoes lysis leading to bacterial inactivation.
- The symmetric (CH$_2$—) vibration band shift during the TiO$_2$ mediated photocatalysis was used as a tool to monitor the progressive disorder in the *E. coli* wall cell bilayers.
- The shift in the symmetric (CH$_2$—) vibration band during photocatalysis seems to be the precursor of the structural changes in the *E. coli* cell-wall bilayers leading to bacterial inactivation in the later stages of the photocatalysis.

- Only a small amount of the bilayer functional groups needs to undergo peroxidation to increase the bilayer wall disorder. This in turn increases the wall fluidity leading to bacterial lysis.

References

[1] T. Matsunaga, R. Tomoda, T. Nakashima, N. Nakamura, T. Tomone, Appl. Environ. Microbiol. 154 (1988) 1330–1337.
[2] P. Maness, S. Smolinski, D. Blake, Z. Huang, E. Wolfrum, W. Jacoby, Appl. Environ. Microbiol. 65 (1999) 4094–4098.
[3] K. Sunada, Y. Kikuchi, K. Hashimoto, A. Fujishima, Environ. Sci. Technol. 32 (1998) 726–729.
[4] D. Gumy, C. Pulgarin, C. Morais, P. Bowen, J. Kiwi, Appl. Catal. B 63 (2005) 76–84.
[5] A.G. Rincon, C. Pulgarin, Appl. Catal. B 44 (2003) 263–270.
[6] G. Rincon, C. Pulgarin, Appl. Catal. B 49 (2004) 99–112.
[7] G. Rincon, C. Pulgarin, Appl. Catal. B 51 (2004) 283–302.
[8] R. Bacsa, J. Kiwi, T. Ohno, P. Albers, V. Nadtochenko, J. Phys. Chem. B 109 (2005) 5994–6003.
[9] J.A. Rengifo-Herrera, E. Mielczarski, J. Mielczarski, N.C. Castillo, J. Kiwi, C. Pulgarin, Appl. Catal. B 84 (2008) 448–456.
[10] J.A. Rengifo-Herrera, A. Sienkiewicz, L. Forró, J. Kiwi, J.E. Moser, C. Pulgarin, J. Phys. Chem. C 114 (2010) 2717–2723.
[11] L.A.P. Brook, P. Evans, H.A. Foster, M.E. Premble, A. Steele, D.W. Sheel, H.M. Yates, J. Photochem. Photobiol. A 187 (2007) 53–63.
[12] K. Page, R. Palgrave, I. Parkin, M. Wilson, S.L.P. Savin, A. Chadwick, J. Mater. Chem. 17 (2007) 95–104.
[13] H.M. Yates, L.A. Brook, I.B. Ditta, P. Evans, H.A. Foster, D.W. Sheel, A. Steele, J. Photochem. Photobiol. A 197 (2008) 197–205.
[14] H.A. Foster, D.W. Sheel, P. Sheel, P. Evans, S. Varghese, N. Rutschke, H.M. Yates, J. Photochem. Photobiol. A 216 (2010) 283–289.
[15] P.M.S. Dunlop, C.P. Sheeran, J.A. Byrne, M.A.S. McMahon, M.A. Boyle, K.G. McGuigan, J. Photochem. Photobiol. A 216 (2010) 303–310.
[16] J. Kiwi, V. Nadtochenko, J. Phys. Chem. B. 108 (2004) 17675–17684.
[17] V. Nadtochenko, A. Rincon, S. Stanka, J. Kiwi, J. Photochem. Photobiol. A 169 (2005) 131–137.
[18] J. Kiwi, V. Nadtochenko, Langmuir 21 (2005) 4631–4641.
[19] V. Nadtochenko, C. Pulgarin, P. Bowen, J. Kiwi, J. Photochem. Photobiol. A 181 (2006) 401–414.
[20] D. Naumann, in: R.A. Meyers (Ed.), Microbiology Encyclopedia of Analytical Chemistry, John Willey & Sons Ltd., Chichester, 2000, pp. 102–131.
[21] V.-M. Mathieu, P. Primet, P. Pichat, J. Phys. Chem. 75 (1971) 1216–1220.
[22] G. Vedantham, G.H. Sparks, U.S. Sane, S.M. Tzannis, T. Przybycien, Anal. Biochem. 33 (2000) 285–292.
[23] C. Selle, W. Pohle, H. Fritzsche, J. Mol. Struct. 480–481 (1999) 401–410.
[24] D. Naumann, C. Schultz, A. Sabisch, M. Kastowsky, H. Labischinsi, J. Mol. Struct. 214 (1989) 213–221.
[25] H.H. Mantsch, R.N. McElhaney, Chem. Phys. Lipids 57 (1991) 213–226.